Strong evidence of normal heat conduction in a one-dimensional quantum system

View the article online for updates and enhancements.

You may also like

Strong evidence of normal heat conduction in a one-dimensional quantum system

K. Saito

Department of Applied Physics, School of Engineering
University of Tokyo - Bunkyo-ku, Tokyo 113-8656, Japan

Abstract. – We investigate how the normal energy transport is realized in one-dimensional quantum systems using a quantum spin system. The direct investigation of local energy distribution under thermal gradient is made using the quantum master equation, and the mixing properties and the convergence of the Green-Kubo formula are investigated when the number of spin increases. We find that the autocorrelation function in the Green-Kubo formula decays as $\sim t^{-1.5}$ to a finite value which vanishes rapidly with the increase of the system size. As a result, the Green-Kubo formula converges to a finite value in the thermodynamic limit. These facts strongly support the realization of Fourier heat law in a quantum system.

The Fourier heat law is one of the most important properties in nonequilibrium thermodynamics. It states that the heat current per volume is proportional to the thermal gradient. The microscopic dynamical origin for the realization of the Fourier heat law has been actively studied using many Hamiltonian systems [1–3]. In the complete harmonic chain, no global thermal gradient appears, and local equilibrium is not realized, which is attributed to the lack of scattering between modes [1, 4]. In an isotropic d-dimensional classical Fermi-Pasta-Ulam (FPU) system which has the nonlinear potential term, the mixing property is satisfied because the auto-correlation function of the energy current roughly decays as $t^{-d/2}$. However, due to the slow relaxation of the current fluctuation, the Green-Kubo formula diverges in the one- and two-dimensional systems, which causes an anomalous energy transport [2, 5].

In low-dimensional systems, most of the problems preventing a normal thermal conduction arise from a slow fluctuation of energy current, including the failure of the mixing property. This situation is also the case in quantum systems. Many integrable one-dimensional systems show the failure of the mixing property. In the isotropic Heisenberg chain, the energy current operator commutes with the Hamiltonian, which trivially causes the failure of the mixing property and the abnormal energy transport [6]. Recent experiments confirmed such ballistic heat transport in Sr_2CuO_3 [7] and $CuGeO_3$ [8] which is described by the isotropic Heisenberg chain.

In this paper, we study how the normal thermal conduction in a one-dimensional quantum system is realized from the microscopic point of view. In quantum systems, the dynamical

origins of normal thermal conduction and the related quantum effects are not enough understood [3,9]. In classical systems, *chaos* characterized by the sensitivity to the initial state can be induced by nonlinearities and can play a crucial role for the mixing property. However, such *chaos* cannot be induced by a linear Schrödinger equation in quantum systems [10]. In spite of such discrepancies in dynamics, the Fourier heat law can be realized in quantum systems. We show strong evidence of the normal thermal conduction in a one-dimensional quantum spin system by direct investigation of properties under thermal gradient and the Green-Kubo formula. We find that the autocorrelation function in the Green-Kubo formula approximately decays as $t^{-1.5}$. Thus the mixing property is satisfied and the formula converges.

We consider the tractable simple quantum system whose Hamiltonian is described as

$$\mathcal{H} = \sum_{\ell=1}^{N_1} J\sigma_\ell^z \sigma_{\ell+1}^z + D\big(\sigma_\ell^z \sigma_{\ell+1}^x - \sigma_\ell^x \sigma_{\ell+1}^z\big) + \Gamma \sum_{\ell=1}^{N} \sigma_\ell^x + H \sum_{\ell=1}^{N} \sigma_\ell^z, \qquad (1)$$

where σ_ℓ^α ($\alpha = x, y, z$) is the α-component of the Pauli matrix at the ℓ-th site. N is the number of spin, and N_1 is taken as $N-1$ for the open boundary condition and N for the periodic boundary condition, respectively. The first term is the nearest-neighbor Ising interaction, and the second term is the Dzyaloshinsky-Moriya (DM) interaction, where the anisotropic vector is taken as $\boldsymbol{D} = (0, D, 0)$ for the general form $\boldsymbol{D} \cdot (\boldsymbol{\sigma}_\ell \times \boldsymbol{\sigma}_{\ell+1})$. The third and fourth terms are the Zeeman term of x- and z-direction, respectively.

This Hamiltonian shows the variety of symmetries by controlling parameters (J, D, Γ, H). In the case of periodic boundary condition, there exists the translational symmetry $\sigma_n \leftrightarrow \sigma_{n+\ell}$ ($\ell = 1, \ldots, N$). In the absence of the DM interaction, *i.e.* $D = 0$, the system has the reflection symmetry, $\sigma_n \leftrightarrow \sigma_{N-n}$. In the case of $D = 0$ and $H = 0$, the system Hamiltonian is diagonalized by using free fermions through the Jordan-Wigner transformation [11]. When $\Gamma = 0$ and $H = 0$, the system has the time-reversal symmetry which yields the Kramers degeneracies. In many systems with symmetries, conserved quantities prevent a normal heat transport, so that the Green-Kubo formula diverges [6,12].

As is well known, the level spectrum shows the universal statistics according to the nonintegrability of the system [13]. We investigate the cumulative spacing distribution $I(S)$ defined by $I(S) = \int_0^S \mathrm{d}u P(u)$ for the energy spacing distribution $P(u)$. We show the distributions in fig. 1 for $(J, D, \Gamma, H) = (0.2, 0.2, 0.2, -0.2)$ and $(0.2, 0, 0.2, 0)$ with the open boundary condition $N_1 = N-1$. The former system has no trivial symmetries, while the latter can be mapped into free fermion. The points are numerical data obtained by diagonalizing the Hamiltonian (1), and the lines are theoretical predictions, *i.e.*, the Poisson distribution $I(S) = 1 - \exp[-S]$ for integrable systems, and the Wigner distribution $I(S) = 1 - \exp[-\pi S^2/4]$ for nonintegrable systems, respectively. The figure for the parameters $(0.2, 0.2, 0.2, -0.2)$ shows the agreement between the numerical data and the Wigner surmise. For small spacing $S \ll 1$, $I(S)$ behaves as $I(S) \propto S^{1.92 \pm 0.02}$, which is very close to the Wigner distribution $I(S) \propto S^2$. This universal feature of the spectrum indicates a complex dynamics of this system. Thus throughout this paper, we take the parameters as $J = D = \Gamma = -H = 0.2$ [14].

In order to investigate properties of the energy transport under thermal gradient, the reservoirs of different temperatures are directly connected with the system at both ends. Here we adopt the phonon reservoir with the Ohmic spectral density for which the master equation of the system is written as (see, *e.g.*, [4] and references therein)

$$\frac{\partial \rho(t)}{\partial t} = -i\big[\mathcal{H}, \rho(t)\big] - \lambda\big(\mathcal{L}_\mathrm{L}\rho(t) + \mathcal{L}_\mathrm{R}\rho(t)\big), \qquad (2)$$

where the first term on the right-hand side corresponds to the pure quantum dynamics of
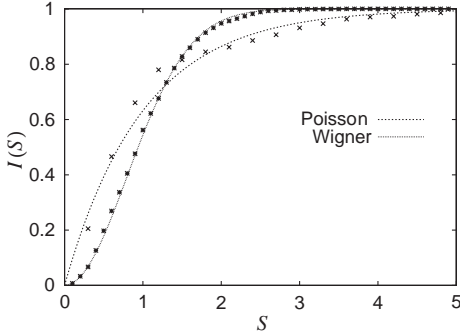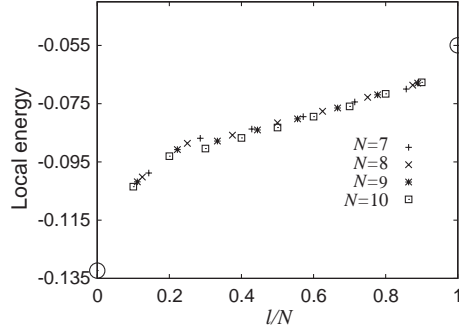
Fig. 1

Fig. 2

Fig. 1 – Cumulative level spacing distribution for $N = 12$ with the open boundary condition. The asterisk and cross are for the cases of $(J, D, \Gamma, H) = (0.2, 0.2, 0.2, -0.2)$ and $(0.2, 0, 0.2, 0)$, respectively. For small S in the former case, $I(S)$ is approximately fitted by $I(S) \propto S^{1.92 \pm 0.02}$.

Fig. 2 – The energy profile at the stationary state for $N = 7, 8, 9, 10$. The abscissa is the scaled spin number, l/N, $l = 1, \ldots, N-1$.

the system, and $\mathcal{L}_{\rm L}$ and $\mathcal{L}_{\rm R}$ express the dissipative effects of the inverse temperature $\beta_{\rm L}$ at the left reservoir and $\beta_{\rm R}$ at the right reservoir, respectively. The parameter λ is the coupling strength. The dissipative term $\mathcal{L}_\alpha$ ($\alpha = {\rm L, R}$) is given by $\mathcal{L}_\alpha \rho(t) = ([X_\alpha, R_\alpha \rho(t)] + [X_\alpha, R_\alpha \rho(t)]^\dagger)$, where $X_{\rm L}$ and $X_{\rm R}$ are the system's operators directly attached to the left and right reservoir, respectively. Here we take $X_{\rm L} = \sigma_1^z$ and $X_{\rm R} = \sigma_N^z$. The operator R_α is given by $\langle k | R_\alpha | m \rangle = (E_k - E_m)(e^{\beta_\alpha(E_k - E_m)} - 1)^{-1} \langle k | X_\alpha | m \rangle$ in the representation diagonalizing the Hamiltonian (1) as $\mathcal{H}|k\rangle = E_k|k\rangle$ and $\mathcal{H}|m\rangle = E_m|m\rangle$.

We first consider the energy profile defining the ℓ-th local Hamiltonian $\mathcal{H}_\ell$,

$$\mathcal{H}_\ell = J\sigma_\ell^z \sigma_{\ell+1}^z + D\big(\sigma_\ell^z \sigma_{\ell+1}^x - \sigma_\ell^x \sigma_{\ell+1}^z\big) + \sum_{k=\ell}^{\ell+1} \big(\Gamma \sigma_k^x + H \sigma_k^z\big). \tag{3}$$

We numerically integrate eq. (2) and obtain the stationary density matrix $\rho_{\rm st}$ when the initial density matrix is taken as the canonical distribution of temperature $1/\beta_{\rm R}$. The simulation was carried out by the fourth-order Runge-Kutta method with the time step 0.01 for the parameters $\beta_{\rm L} = 0.5$, $\beta_{\rm R} = 0.2$, and $\lambda = 0.01$. In fig. 2, we show the energy profiles at the stationary state $\mathrm{Tr}(\rho_{\rm st} \mathcal{H}_\ell)$ for $N = 7, 8, 9,$ and 10. The two large circles are equilibrium energy values of inverse temperatures $\beta_{\rm L}$ and $\beta_{\rm R}$, respectively. $N = 10$ was the largest number within the present computational ability. The figure shows the profiles with a finite gradient which is the *sufficient condition* for the Fourier heat law, although we cannot enumerate the energy profile and energy current in the thermodynamic limit. The local energies at both edges are different from the expectation values of the temperatures of reservoirs. This is attributed to the small coupling strength λ (= 0.01). Actually, we confirmed that for larger λ ($\ll J, D$), the energy profile smoothly changes and these differences become smaller. We found the qualitatively same finite energy gradient in the case of smaller temperature difference $\beta_{\rm L} = 0.3$ and $\beta_{\rm R} = 0.2$.

We next study the local energy distribution at the stationary state focusing on whether the local equilibrium is realized or not for the system of $N = 10$. The local equilibrium can be realized even in finite-size systems [15, 16]. We study the energy distribution of subsystems
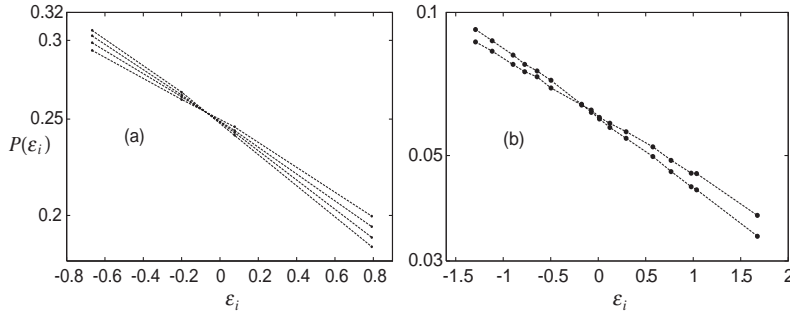
Fig. 3 – Local energy distribution for size $N = 10$. (a) Four local subsystems composed of two spins for $(\beta_{\mathrm{L}}, \beta_{\mathrm{R}}) = (0.5, 0.2)$. (b) Two local subsystems composed of four spins for $(\beta_{\mathrm{L}}, \beta_{\mathrm{R}}) = (0.3, 0.2)$.

composed of two spins and four spins. We consider four local subsystems with two spins, *i.e.*, the subsystems described by the local Hamiltonians, $\mathcal{H}_2, \mathcal{H}_4, \mathcal{H}_6$, and $\mathcal{H}_8$, and two local subsystems with four spins, *i.e.*, the subsystems described by $(\mathcal{H}_2 + \mathcal{H}_3)$ and $(\mathcal{H}_6 + \mathcal{H}_7)$. Temperatures at boundaries are set as $(\beta_{\mathrm{L}}, \beta_{\mathrm{R}}) = (0.5, 0.2)$ for the former case and $(\beta_{\mathrm{L}}, \beta_{\mathrm{R}}) = (0.3, 0.2)$ for the latter case. The ℓ-th local energy distribution $P_\ell(\varepsilon_i)$ is calculated using the ℓ-th local reduced density matrix ρ_ℓ as

$$P_\ell(\varepsilon_i) \;=\; \langle i_\ell | \rho_\ell | i_\ell \rangle, \tag{4}$$

where $|i_\ell\rangle$ is the i-th eigenstate of the ℓ-th local subsystem Hamiltonian. The numbers of eigenstates are 4 and 16 for the cases of $(\beta_{\mathrm{L}}, \beta_{\mathrm{R}}) = (0.5, 0.2)$ and $(\beta_{\mathrm{L}}, \beta_{\mathrm{R}}) = (0.3, 0.2)$, respectively. The ℓ-th local density matrix ρ_ℓ is obtained by taking the trace for stationary density matrix ρ_{st} in the Hilbert space exclusive of spins which belong to the ℓ-th subsystem. In fig. 3, the energy distributions $P_\ell(\varepsilon_i)$ are shown on the semi-log scale. The points linked by one line are the distribution at one local subsystem. With the increase of the subsystem number ℓ, the gradient of the line becomes smaller. The distributions approximately take the exponential form. Thus this monotonic ℓ-dependence of the gradient of energy distribution indicates that this system can be the *candidate* which satisfies the local equilibrium. We must note that the Ising and DM interaction between nearest-neighbor local subsystems and the existence of finite energy flow can cause deviations of $P_\ell(\varepsilon_i)$ from the exponential form.

Generally, even if the energy profile is well scaled and the local equilibrium is realized, thermal conductivity can diverge in the thermodynamic limit due to the slow relaxation of energy currents mentioned in the introduction [16]. We now investigate whether this type of divergence occurs or not in the present system. The Green-Kubo formula is derived on the basis of the local equilibrium state. Since the present system is the candidate which satisfies the local equilibrium, we expect that the Green-Kubo formula quantitatively describes the thermal conductivity $\kappa(\beta)$ in the thermodynamic limit. The Green-Kubo formula reads as

$$\kappa(\beta) \;=\; \frac{\beta^2}{2N} \int_0^\infty \mathrm{d}u \langle \{\hat{J}, \hat{J}(u)\} \rangle, \tag{5}$$

where $\{\cdot, \cdot\}$ means the anti-commutation relation, and $\langle \ldots \rangle$ is the equilibrium average at the inverse temperature β. The operator $\hat{J}(u)$ is the total current operator at the time u in the Heisenberg picture, *i.e.*, $\hat{J}(u) = \exp[i\mathcal{H}u]\hat{J}\exp[-i\mathcal{H}u]$. The total current operator $\hat{J}$ is calculated by the continuity equation of energy as $\hat{J} = -i\sum_\ell([\hat{h}_{\ell+1}, \hat{h}_\ell] + [\hat{h}_{\ell+2}, \hat{h}_\ell])$, using
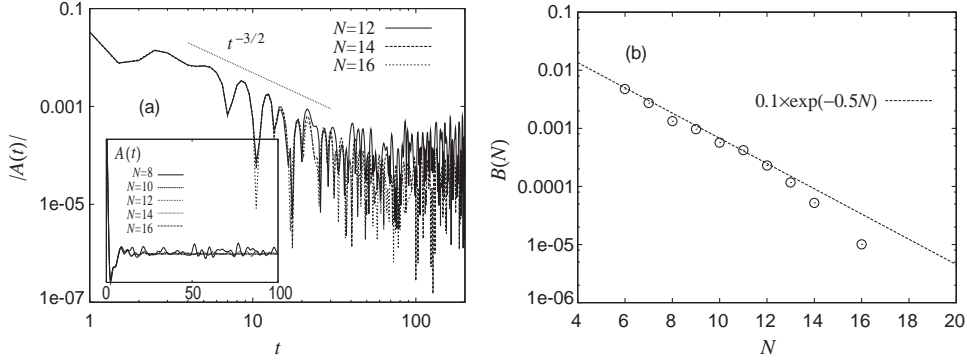
Fig. 4 – (a) The absolute values of the autocorrelation function as a function of time for $N = 12, 14$ and 16. In the inset, the raw data are shown for $N = 8, 10, 12, 14$ and 16. (b) The average constant $B(N)$ as a function of N. The dashed line is the exponential function $0.1 \times \exp[-0.5 \times N]$.

$\hat{h}_\ell = J\sigma_\ell^z \sigma_{\ell+1}^z + D(\sigma_\ell^z \sigma_{\ell+1}^x - \sigma_\ell^x \sigma_{\ell+1}^z) + \Gamma\sigma_\ell^x + H\sigma_\ell^z$. In order to consider the thermodynamic limit, we define $A(t)$ and $C(t)$ as follows:

$$A(t) = \frac{1}{2N}\langle\{\hat{J}, \hat{J}(t)\}\rangle, \qquad C(t) = \int_0^t \mathrm{d}u A(u), \tag{6}$$

where $A(t)$ is the autocorrelation function for the total current, and $C(t)$ is the integration of $A(t)$. We call $C(t)$ the Green-Kubo integral. The numerical calculations are carried out for $\beta = 0.3$ with the periodic boundary condition $N_1 = N$. In fig. 4(a), we plotted the absolute values of the autocorrelation functions $A(t)$ for system sizes $N = 12, 14$ and 16 on the log-log scale. Up to $N = 14$, we used the numerical diagonalization for the Hamiltonian, and for $N = 16$ we calculated the time evolution of wave function for the randomly chosen 1024 initial states [9]. The figure indicates the power law decay $\sim t^{-1.5}$ of $A(t)$. In the inset, the raw data of $A(t)$ for various system sizes ($N = 8, 10, 12, 14$, and 16) are plotted on the normal scale. All data are saturated to some finite values with fluctuations. This constant is partially caused by the energy degeneracies due to translational symmetry of periodic condition. Thus the behavior of $A(t)$ is roughly represented as follows:

$$A(t) \sim a(N,t)t^{-1.5} + b(N,t) + B(N), \tag{7}$$
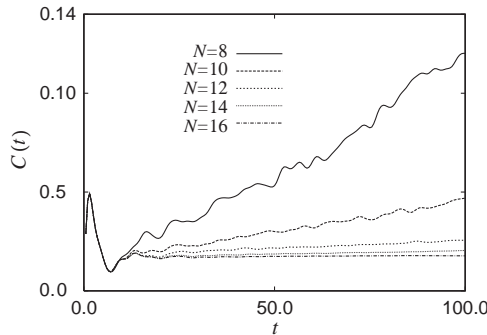

Fig. 5 – The Green-Kubo integral $C(t)$ as a function of time for $N = 8, 10, 12, 14$ and 16.

where $a(N, t)$ and $b(N, t)$ are some fluctuating functions with a vanishing mean value and $B(N)$ denotes the saturated average value for N. $B(N)$ can be exactly calculated by a numerical diagonalization up to $N = 14$. For $N = 16$, it is calculated by directly averaging the numerical data of $A(t)$. We find that $B(N)$ vanishes with the increase of N following or faster than the exponential function $0.1 \times \exp[-0.5N]$, as shown in fig. 4(b). There we plotted the data from $N = 6$ to $N = 16$. Thus the integral $C(t)$ is expected to converge showing roughly the following behavior in the thermodynamic limit $N \to \infty$:

$$C(t) \sim \int^t a(N, u) u^{-1.5}\, \mathrm{d}u + B(N) t \longrightarrow \int^t a(\infty, u) u^{-1.5}\, \mathrm{d}u < C_0 + t^{-0.5}. \qquad (8)$$

In fig. 5, we present the numerically calculated $C(t)$ for various N. The behavior of $C(t)$ strongly supports the convergence of the Green-Kubo integral in the thermodynamic limit. The behavior of $C(t)$ reminds us of the order of limit, *i.e.*, taking the limit N to infinity first and then t to infinity. From the convergence of $C(t)$, we conclude that the present one-dimensional spin system without trivial symmetries shows the finite thermal conductivity which is independent of the system size as far as N is very large.

In conclusion, we find strong evidence of normal thermal conduction in the present system by microscopic investigation. The autocorrelation function in the Green-Kubo formula shows the power law decay $\sim t^{-1.5}$, which may be characteristic in the high-temperature region, *i.e.* the semiclassical region [17]. It is also interesting to study the behavior at very low temperatures. Figure 3 indicates that this system can be the candidate which satisfies the local equilibrium. We should carefully and systematically investigate how the exponential form in the local energy distribution is realized.

In the recent experiments showing a ballistic heat transport in Sr_2CuO_3 [7] and $CuGeO_3$ [8], the energy is transmitted by spin excitations (magnon), and the coherent length is very long (about 100 times lattice constant in $CuGeO_3$ above the spin-Peierls temperature). Theoretical studies for the temperature dependence of thermal conductivity are actively done [18, 19]. It is also interesting to investigate theoretically and experimentally how the coherent length changes when the symmetries disappear in these realistic systems.

$$* * *$$

REFERENCES

[1] Rieder Z., Lebowitz J. L. and Lieb E., *J. Math. Phys.*, **8** (1967) 1073; Zürcher U. and Talkner P., *Phys. Rev. A*, **42** (1990) 3278.
[2] Lepri S., Livi R. and Politi A., *Phys. Rev. Lett.*, **78** (1997) 1896; *Europhys. Lett.*, **43** (1998) 271.
[3] Saito K., Takesue S. and Miyashita S., *Phys. Rev. E*, **54** (1996) 2404.
[4] Saito K., Takesue S. and Miyashita S., *Phys. Rev. E*, **61** (2000) 2397.
[5] Lippi A. and Livi R., *J. Stat. Phys.*, **100** (2000) 1147; Shimada T., Murakami T., Yukawa S., Saito K. and Ito N., *J. Phys. Soc. Jpn.*, **69** (2000) 3150.

[6] MAZUR P., *Physica*, **43** (1969) 533; ZOTOS X., NAEF F. and PRELOVSEK P., *Phys. Rev. B*, **55** (1997) 11029.

[7] SOLOGUBENKO A. V., GIOANNÓ K., OTT H. R., VIETKINE A. and REVCOLEVSCHI A., *Phys. Rev. B*, **62** (2000) R6108; **64** (2001) 054412-1.

[8] ANDO Y., TAKEYA J., SISSON D. L., DOETTINGER S. G., TANAKA I., FEIGELSON R. S. and KAPITULNIK A., *Phys. Rev. B*, **58** (1998) R2913.

[9] PROSEN T., *Phys. Rev. Lett.*, **80** (1998) 1808; *Phys. Rev. E*, **60** (1999) 3949.

[10] JONA-LASINIO G. and PRESILLA C., *Phys. Rev. Lett.*, **77** (1996) 4322.

[11] KATSURA S., *Phys. Rev.*, **127** (1962) 1508.

[12] For example, in the free fermion case of $D = H = 0$, the fermion can run through without scatterings, which causes the ballistic transport. In that case, the temperature profile becomes flat [3].

[13] BOHIGAS O., GIANNONI M.-J. and SCHMIT C., *Phys. Rev. Lett.*, **52** (1984) 1; BERRY M. V. and TABOR M., *J. Phys. A*, **10** (1977) 371.

[14] We regard the system (1) as a dynamical model which shows a variety of complex dynamics. We take this simple set of parameters although the DM interaction is relatively large.

[15] SAITO K., TAKESUE S. and MIYASHITA S., *Phys. Rev. E*, **59** (1999) 2783.

[16] DHAR A., *Phys. Rev. Lett.*, **86** (2001) 3554.

[17] PROSEN T., *Prog. Theor. Phys. Suppl.*, **139** (2000) 191.

[18] KLÜMPER A. and SAKAI K., *J. Phys. A*, **35** (2002) 2173.

[19] SAITO K. and MIYASHITA S., *J. Phys. Soc. Jpn.*, **71** (2002) 2485.